Unraveling the Formation Mechanism of a Hybrid Zr-Based Chemical Conversion Coating with Organic and Copper Compounds for Corrosion Inhibition

Xiaoyang Liu, Donald Vonk, Kim Kisslinger, Xiao Tong, Gary Halada, Stanislas Petrash, Kate Foster, and Yu-chen Karen Chen-Wiegart*

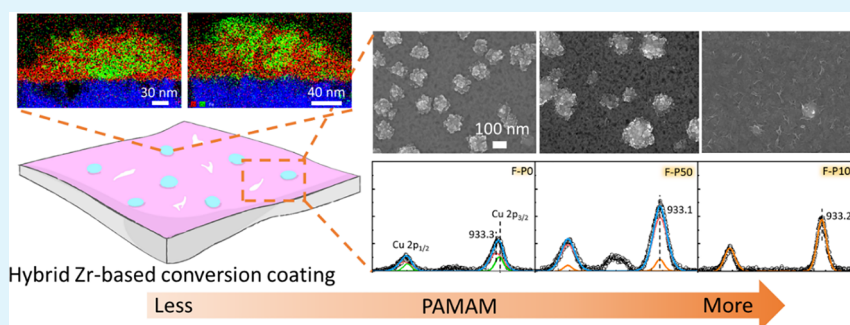Cite This: https://dx.doi.org/10.1021/acsami.0c19203

Read Online

ACCESS | Metrics & More | Article Recommendations | Supporting Information

ABSTRACT: Environmentally friendly chromate-free, zirconium (Zr)-based conversion coating is a promising green technology for corrosion protection. Additives in the surface treatment provide critical functionalities and performance improvements; however, mechanistic understanding as to how the additives influence the coatings remains unclear. In this study, a new organic–inorganic hybrid Zr-based conversion coating combines copper (Cu) compounds and polyamidoamine (PAMAM), taking advantage of the complementary nature of organic and inorganic additives. A multimodal approach combining electron and X-ray characterization is applied to study the interaction of Cu^{2+} and PAMAM and the resulting impacts on coating formation. Adding PAMAM changed the surface morphology, thickness, distribution of Cu in the clusters, and void formation of the coatings. High PAMAM (100−200 ppm) leads to little conversion coating formation, and low PAMAM (0−25 ppm) shows voids formation under the coatings. Moreover, PAMAM incorporates in the coating in the form of a PAMAM−Cu complex with a higher concentration toward the surface, providing an organic layer at the surface of the coating. X-ray absorption near-edge structure (XANES) spectroscopy shows the difference between the conventional and the hybrid coating treatments in an alkaline solution to simulate the E-coat process, suggesting the contribution of PAMAM in the enhanced chemical stability in an alkaline environment. Therefore, an intermediate range of addition of PAMAM (50 ppm) is optimal to (1) avoid excessive voids formation, (2) promote some Cu cluster formation and thus enhance the Zr-based coating formation, and (3) incorporate organic components into the coating to improve the adhesion of the subsequent coatings. Overall, this work furthers our knowledge on the formation mechanism of an effective and environmentally friendly hybrid conversion coating for corrosion inhibition, demonstrating a critical processing−structure−property relationship. This study will benefit future development of green and effective surface treatment technology.

KEYWORDS: conversion coating, surface treatment, coating growth, XPS, metal−organic

1. INTRODUCTION

Corrosion is one of the main destructive processes on metals and alloys leading to great economic, health, and ecological losses.[1] Corrosion prevention technologies including cathodic protection, protective coatings, and corrosion inhibitor are thus essential and have pervasive impacts in a wide range of industries.[2−4] Deposition of a thin chemical conversion coating on a metallic surface via a simple solution immersion process as a pretreatment is convenient and economic with applications in automotive, aerospace, and energy storage.[5,6] The resulting conversion coatings could provide an effective barrier for corrosion prevention and improve the adhesion between the metal and the subsequent organic coating.[7] However, conventional chromate coatings contain hexavalent chromium species which are toxic and carcinogenic. Phosphate conversion

coatings contain tricationic phosphate species which cause an eutrophication issue in fresh water; as a result, it can be costly with high energy consumption to process the waste.[8] Both chromate and phosphate conversion coatings have been prohibited or restricted for use in recent years.[9,10] Therefore, there is strong motivation to study and design a novel environmentally friendly chemical conversion coating with both green chemistry and better anticorrosion and adhesion properties.

Prior research studied different green alternatives including rare-earth-based, vanadate-based, lithium-containing, zirconium-based coatings and nanocomposites.[11] Only a few of the investigated systems could be mature enough to be commercialized. Specifically, a zirconium (Zr)-based conversion coating becomes an outstanding alternative to the conventional coatings and has been utilized in various applications with a potential to lower operational cost in the area of energy, maintenance, and reducing the environmental impacts.[12,13] The typical deposition processing methods of the Zr-based conversion coating are the spray method or immersion in a hexafluorozirconic acid (H_2ZrF_6) solution. Previous research focused on improving the anticorrosion performance by controlling the coating deposition parameters including temperature, time, pH, pretreatment on the substrate surface, and adding other compounds as additives in the conversion solution.[14−16]

In particular, the additives in the conversion coating solution could improve the corrosion prevention and adhesion properties of the coatings. Studies have investigated the coating formation mechanism and the functionality of different inorganic additives, for example, copper (Cu), vanadium, or cerium ions on various metal substrates.[17,18] In addition, other studies incorporated organic compounds in the conversion coating solutions aiming to improve the adhesion to the substrate and homogeneity of the coating as well as to provide a base for subsequent organic coatings such as poly(acrylic acid).[12] These studies motivated the idea to simultaneously add inorganic and organic additives, forming a "hybrid-conversion coating", to provide advantageous characteristics of both inorganic and organic additives.[19,20] Specifically, the Zr-based conversion coating with Cu^{2+} additive has been studied from previous works, indicating the function of Cu^{2+}, the elemental distribution in the coating, and the corrosion resistance improvements on cold rolled steel substrate.[8,28] However, studies on the interface morphology between the coating and the substrate, the morphology of the Cu in the coating, and the influence of the interaction between organic compounds and Cu^{2+} on the coating formation mechanism have not been performed in detail. However, incorporating multiple additives could impact the coatings' chemistry and morphology in a complex way. The solubility, compatibility, reactions, and relative ratio of different additives will significantly influence the coating growth mechanism. Hence, it is important to understand the change of reactions for coating formation by systematically investigating the influence of hybrid additive compounds.

In this work, we studied a novel hybrid Zr-based conversion solution consisting of polyamidoamine (PAMAM) containing amide and amine groups and Cu^{2+} ions. The hybrid Zr-based conversion coatings showed better corrosion resistance in the General Motors Worldwide test 14872 exposure C (GMW14872) cyclic corrosion laboratory test, 10-day hot salt water soak corrosion test, and Volkswagen test PV1210 corrosion resistance test (PV1210).[19] Different concentrations (parts per million, ppm) of PAMAM (0, 25, 50, 100, and 200 ppm) were added with a constant concentration of Cu^{2+} ion (10 ppm). The coatings were prepared on iron (Fe) substrates to reflect the wide and important industrial applications of Fe alloys. Specifically, the Fe substrates used in this study included thin films prepared by physical vapor deposition to enable fundamental understanding and higher data quality in characterization. Moreover, the ability to create a conversion coating on Fe thin films may also lead to future applications in a broader area concerning thin film processes.

Herein, this work focuses on studying the interaction between Cu^{2+} ions and PAMAM and their impact on reactions during coating growth with a specific aim to better understand the coating formation mechanism and its associated morphological and chemical evolution. Note that the hybrid conversion coating studied here is chromate free and environmentally friendly. Also noteworthy is that the resulted coatings were characterized by a multimodal approach, combining electron microscopy and X-ray techniques which have been widely utilized in functional materials and fundamental research,[21−23] providing a more comprehensive understanding on the chemical and morphological differences from the Cu−PAMAM coating conditions. The decreasing number density of clusters, thickness, and elemental distribution change because of the coordination complexation between Cu^{2+} and PAMAM were revealed by scanning electron microscopy (SEM), focused ion beam (FIB)-SEM, and high-resolution scanning transmission electron microscopy (STEM). Moreover, the elemental ratio evolution along the depth direction and chemical composition in the coating depending on the amount of PAMAM was observed by X-ray photoelectron microscopy (XPS) with argon (Ar) sputtering depth profiling capability. The mechanism of how PAMAM incorporates into the coating as well as its spatial distribution within the coating (higher toward the surface) are also discussed. Furthermore, to simulate the subsequent application of electrocoating (E-coat) after the conversion coating process, the coating samples were treated repeatedly with several time steps in sodium hydroxide (NaOH) solution and characterized by X-ray absorption near-edge structure (XANES) spectroscopy. Overall, this work introduced the Cu^{2+} and PAMAM hybrid conversion coating with enhanced performance and explained the coating formation mechanism. The results furthered our mechanistic understanding on the hybrid coating formation and will benefit future functional surface coating design and applications.

2. METHODS AND CHARACTERIZATION

2.1. Fe Thin Film Preparation. The thin film preparation process was conducted at the Center for Functional Nanomaterials (CFN) of Brookhaven National Laboratory (BNL). The Fe thin film was prepared by an E-beam evaporator (Kurt J. Lesker PVD 75) on a silicon (Si) wafer. The Si wafer was plasma cleaned first. Fe metal, purity 99.995%, was the source material. The deposition rate was ∼5 Å/s at a high voltage of 7.8 kV under a vacuum of 1×10^{-6} Torr with ∼100 nm film.

Typically, the substrate used in automotive or aerospace applications is carbon (C) steel. However, there will be two drawbacks if one uses engineering alloys to study the reaction mechanisms. First, the magnetic properties of thick carbon steel lead to challenges in high-resolution electron microscopy analysis. In addition, the C signals from carbon steel may mix with the C signals from PAMAM, leading to difficulties to analyze their chemical speciation in spectroscopic analysis. Thus, we used a Fe thin film to mitigate these issues and to investigate the interaction process of the conversion coatings and Fe. Thin films do not

interfere with the electron microscopy analysis as much as the thick substrate, and the pure Fe substrate allows analyzing the C signals from the coating, leading to a better mechanistic understanding for designing controllable coating processes.

2.2. Conversion Coating Solution Preparation. Solutions of the conversion coating were made using different concentrations (parts per million, ppm) of PAMAM (0, 25, 50, 100, and 200 ppm) with a constant concentration of Cu^{2+} ion (10 ppm). The conversion coating solution consists of hexafluorozirconic acid with the Cu added to the solution as cupric nitrate to maintain a zirconium content of 50−300 ppm and a Cu content of 10 ppm in solution. The pH of all solutions was adjusted to pH 4.0. The PAMAM was added to the solutions to obtain different concentrations of PAMAM (0, 25, 50, 100, and 200 ppm). Details of the zirconium-based conversion coating solutions have been previously published.[19,20]

2.3. Deposition of Hybrid Zr-Based Conversion Coating. The Fe thin film or bulk low-carbon steel substrates (cold rolled steel AISI 1008, ACT Test Panels) were immersed in alkaline solution for 120 s at a temperature (T) of 48 °C and rinsed in deionized (DI) water for 60 s at $T \approx 24$ °C. The alkaline solution contains potassium hydroxide, sodium hydroxide, sodium nitrite, and sodium silicate (Bonderite C-AK T51, Henkel Corp., Madison Heights, MI), producing a pH value of 11.7. Then the samples were immersed in different Zr-based conversion solutions at 32 °C for 120 s. The final step was to rinse the samples in DI water for 60 s at $T \approx 24$ °C and to thoroughly dry them by compressed air. The coated samples are listed in Table 1. The coating formation process is shown in Figure 1A.

Table 1. Coating Samples Made of Different Substrates, PAMAM Concentration, and Cu^{2+} Ions Concentration in the Study[a]

sample ID	substrate	PAMAM concentration (ppm)	Cu^{2+}-ion concentration (ppm)
F-P0		0	
F-P25		25	
F-P50	Fe thin film	50	
F-P100		100	10
F-P200		200	
B-P0		0	
B-P50	cold rolled steel	50	
B-P0-noCu		0	0

[a]The sample ID is defined as follows. The substrate types are either Fe film (F) or bulk cold rolled steel (B). The solution may contain varying concentrations of PAMAM (P) in ppm. If not specified in the sample ID, the Cu^{2+} ion concentration used in this study is 10 ppm, except for one comparison sample where no Cu-containing additives were added (noCu).

2.4. NaOH Treatment and XANES. Each coated sample was treated in 0.1 M NaOH solution (pH = 12.5) prepared from NaOH pellets (Alfa Aesar) at 38 °C repeatedly for XANES measurements at different time points of the same sample: 0, 2, 10, and 20 min. At each time point, the sample was characterized at the Beamline for Materials Measurement (BMM) beamline at the National Synchrotron Light Source-II (NSLS-II) of BNL.[24] A grazing incident geometry was used at BMM beamline to increase the surface sensitivity of the measurement. XANES spectra of the Cu K-edge from the samples were collected in fluorescence mode by scanning the monochromator in fluorescence mode. Moreover, Cu foil, CuO, and Cu_2O powders were measured in transmission mode as standards.

2.5. SEM, FIB-SEM, STEM, and XPS Characterization. SEM (JEOL 7600F) was used to characterize the surface morphology of the samples at a 15.0 keV accelerating voltage. FIB-SEM (FEI Helios 600 Nanolab Dualbeam FIB) was used to prepare and characterize the cross-sectional profile of the coatings as well as to prepare cross-sectional TEM samples by a lift-out method. Platinum (Pt) was first deposited as the protective layer prior to the lift-out procedure,

followed by an established protocol, with final gallium ion (Ga^+) milling performed at 5 keV, extracted, and mounting the samples onto a TEM sample holder. STEM was conducted in a TEM (Talos, FEI), operating at 200 keV. High-angle annular dark-field imaging (HAADF) and EDX analysis were carried out to study the elemental distribution at different features on cross-sectional TEM samples. The elemental distribution along the depth direction and chemical composition were characterized by XPS in an ultrahigh-vacuum (UHV) system with a base pressure < 2 × 10^{-9} Torr equipped with a hemispherical electron energy analyzer (SPECS, PHOIBOS 100) and twine anode X-ray source (SPECS, XR50). Al Kα (1486.6 eV) radiation was applied. The angle between the analyzer and the X-ray source was 45°, and photoelectrons were collected at the sample surface normal direction. Argon ion (Ar^+) sputtering with a 500 eV kinetic energy was applied intermittently for layer by layer removal to obtain the elemental atomic ratio and composition as a function of depth relative to the original surface. CasaXPS software was utilized to fit the elements' peak and calculate the atomic ratio. The C 1s peak at 284.8 eV was applied to calibrate the energy shift with Shirley background subtraction. SEM, FIB-SEM, STEM, and XPS measurements were conducted at CFN of BNL.

3. RESULT AND DISCUSSION

3.1. Effect of PAMAM on the Morphology of the Coating. The representative surface and cross-sectional morphologies of pristine Fe thin film are shown in Figure 1A. The Fe thin film has a uniform surface morphology with elongated granular surface features. This surface morphology is similar to what has been reported in the literature by Basnet et al. in their work on Fe_2O_3 thin film. They suggested that a [110] growth direction would be responsible for this type of morphology, supported by detailed X-ray diffraction analysis.[25] Surface XPS suggested that the Fe_2O_3 layer was formed on the surface of the pristine Fe thin film, consistent with the surface morphology, which is similar to the oxidation behavior seen in bulk carbon steel substrates as well (Figure S1). The thickness of the pristine Fe thin film was 135 ± 5 nm. After treatment in different conversion solutions, the top views of the coating samples are shown in Figure 1B. As a control group, sample F-P0 showed round Cu-rich clusters on the surface, which are consistent with the Cu-rich clusters formed on regular low-carbon steel substrates in prior studies.[8,17] With increasing PAMAM concentration, first, at lower PAMAM concentration, for samples F-P25 and F-P50, Cu-rich clusters still formed on the surface of the coating (Figure S2). By quantifying the size and number density of the clusters (Figure S3), the number density of the clusters continuously decreased from 4.2 (F-P0) to 2 μm^{-2} (F-P50). This indicates that less Cu^{2+} ions in the solution reacted to form clusters. However, the diameter of the cluster did not change significantly, which showed that the reaction rate to form clusters from Cu^{2+} ions did not change with the PAMAM concentration during coating formation. Since PAMAM has a high density of functional amine and amide groups, it could chelate with Cu^{2+} ions in the solution, leading to reducing the amount of metallic Cu deposition in the coating.[26,27] Furthermore, when the amount of PAMAM increased to 100 and 200 ppm, clusters no longer formed on the surface of the coating. Instead, a flake-like structure covered the surface, which could indicate that the PAMAM chelates with and consumes the majority of Cu^{2+} ions in solution. Therefore, deposition of the clusters could not occur. In addition, the surface morphology of F-P100 and F-P200 was compared with samples B-P0-noCu (Zr-based solution without both Cu^{2+} ions and PAMAM, Figure S4), and the flake-like structures were only present in F-P100 and F-P200 samples. Thus, this flake-like feature may be from PAMAM, indicating that chelated Cu−
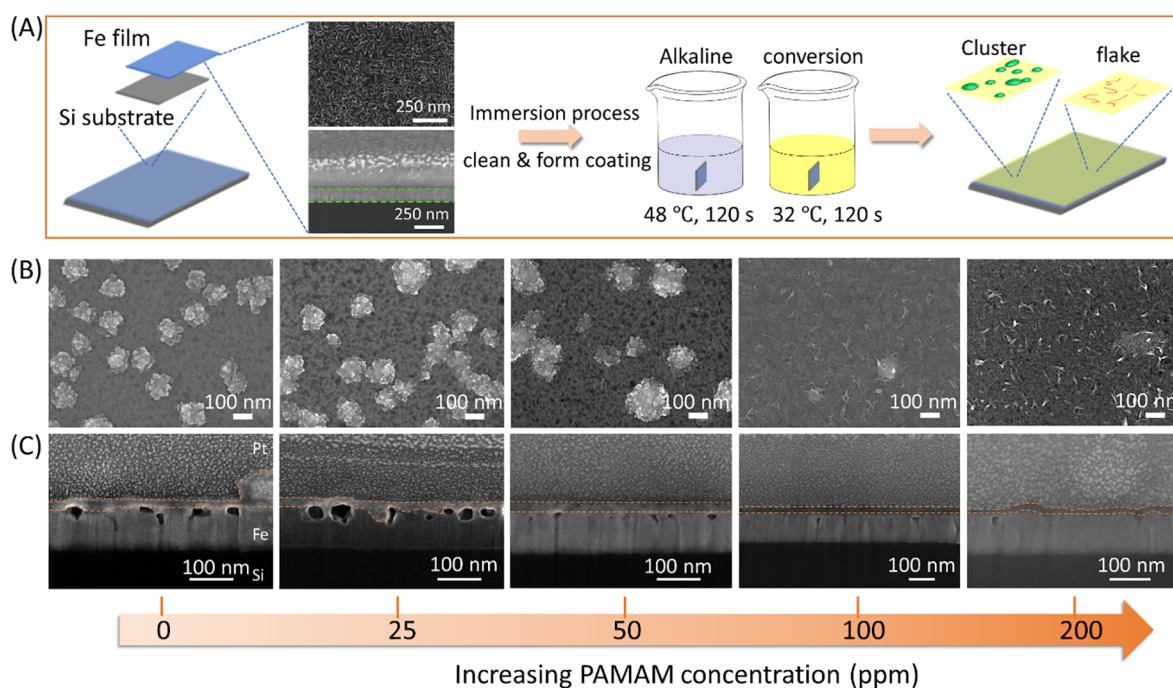
Figure 1. (A) Preparation process of hybrid Zr-based conversion coating on Fe thin film substrates with top and cross-sectional view. Fe layer is indicated by green dashed lines. (B) Surface morphology of different coating samples with increasing PAMAM concentration from 0 to 200 ppm. (C) Cross-sectional profiles of the conversion coatings are indicated by orange dashed lines.
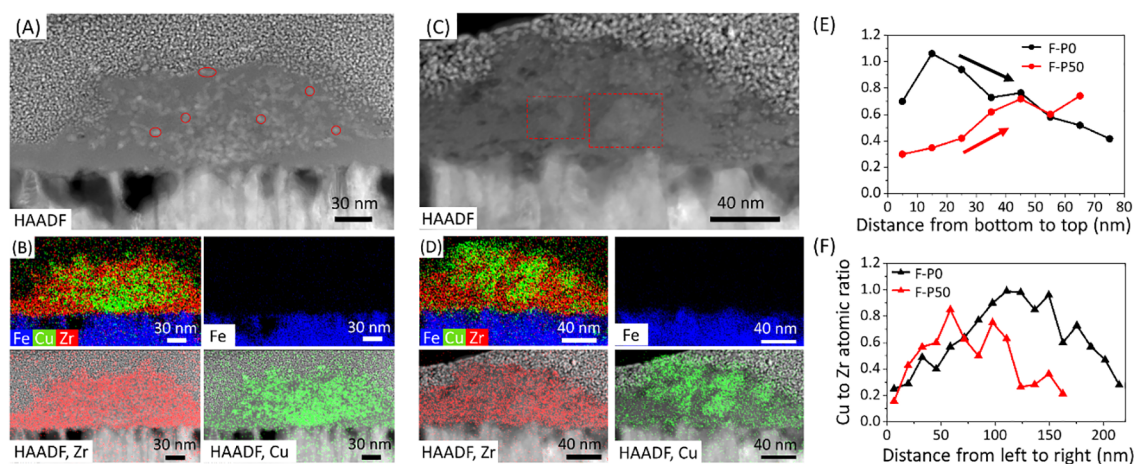

Figure 2. STEM analysis of coatings with 0 and 50 ppm PAMAM (F-P0 and F-P50) showing the morphology and elemental distribution on the cross-sectional cluster region. (A) High-angle annular dark-field image (HAADF) of F-P0; Cu nanoparticles are indicated by red circles. (B) EDX analysis of Fe, HAADF-STEM with Zr, and HAADF-STEM with Cu. (C) HAADF of F-P50, agglomeration of Cu particles is indicated by red dashed frames. (D) EDS maps of Fe, HAADF-STEM with Zr, and HAADF-STEM with Cu. (E) Elemental ratio profile along the vertical direction: Cu to Zr atomic ratio from the bottom to the top of the cluster decreased for F-P0 and increased for F-P50. (F) Elemental ratio profile along the lateral direction: Cu to Zr atomic ratio changes from left to right of the cluster.

PAMAM might still be incorporated into the coating during deposition, which will be discussed in detail below.

In addition to the influence on formation of the clusters, incorporation of PAMAM changed the thickness and voids formation in the coating. Figure 1C shows the cross-sectional view of the coating samples. The thicknesses of F-P0, F-P25, and F-P50 were ~25 ± 5 nm at the region without clusters. However, for samples F-P100 and F-P200, the thicknesses were ~15 ± 5 nm. This suggests that the growth rate of the coating was slower when the PAMAM concentration was higher since the treatment time and temperature were the same for all conditions. Previous research suggested that Cu^{2+} promotes the growth of Zr-based

coating.[28] However, when PAMAM chelated with Cu^{2+} ions in solution, less free Cu^{2+} ions are available to promote the coating reaction. Hence, a lower extent of coating formation was observed. In addition, some voids with varying size were clearly present at the interface between the coating and the Fe thin film substrate for samples F-P0 and F-P25. However, the number and size of the voids gradually decreased with increasing PAMAM concentration, as can be observed in the FIB-SEM images, Figure 1C.

Cerezo et al. characterized a decrease of the open-circuit potential (OCP) during the initial deposition of Zr-based coatings with Cu additives on cold rolled steels, which was
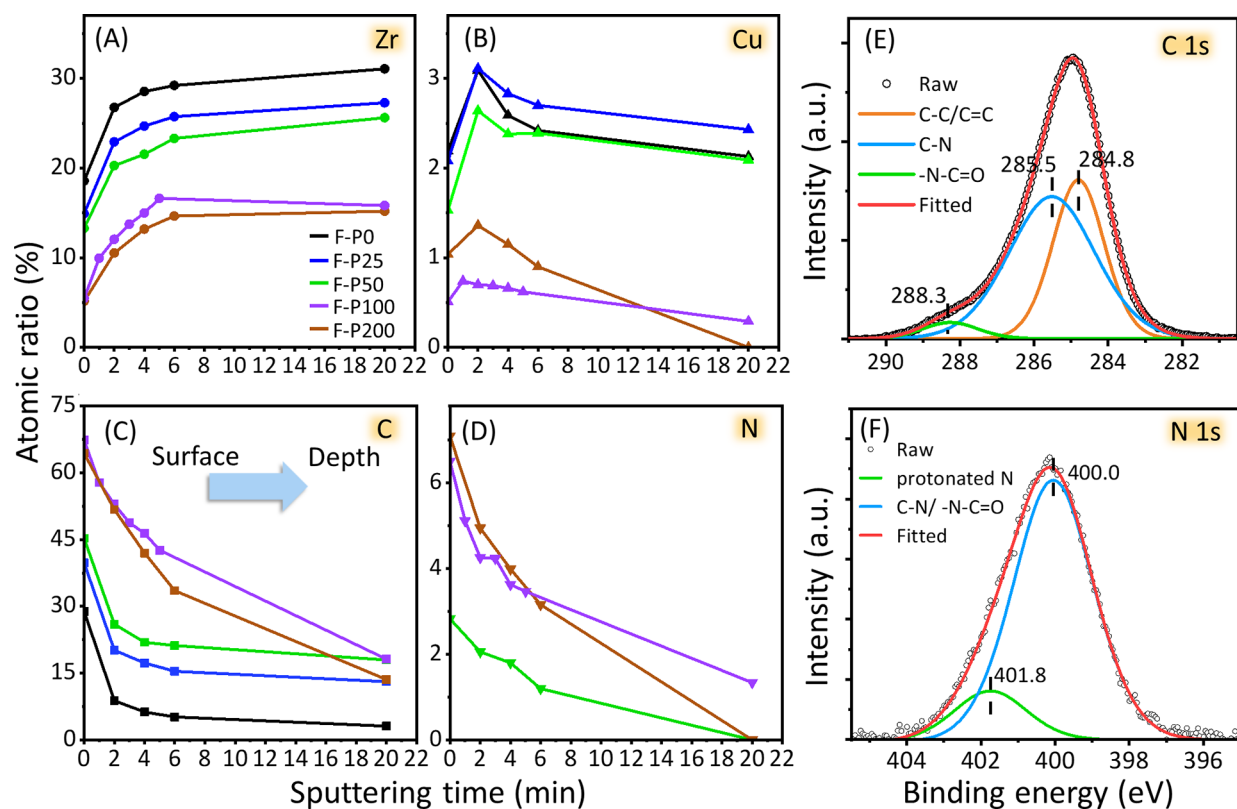
Figure 3. (A−D) Atomic ratio depth profiles of Zr, Cu, C, and N in different samples show the elemental evolution along the depth direction in different coatings. Atomic ratio is determined from XPS peak, and total sum of all analyzed elements (C, N, O, F, Zr, and Cu) for each sample is 100%. Longer sputtering time corresponds to probing deeper regions into the coating. (E and F) C 1s and N 1s XPS of sample F-P100 at the surface.

attributed to the activation of the metal surface with the free F^- ions in solution.[29] The metal surface interaction with F^- ions included replacement of small amounts of O^{2-} ions in the outer part of the surface metal oxides by F^- ions, which would then be easier to dissolve during the conversion coating process.[30] Introducing F^- ions created vacancies in the lattice and increased the transport rate of metal ions. Therefore, as anodic dissolution of the Fe occurred, dissolved Fe ions can diffuse through the surface oxide easier; this anodic dissolution of Fe may be accompanied by voids formation. Meanwhile, when Cu^{2+} is reduced during coating formation, dissolution of Fe as the anodic counter reaction is further promoted. However, the increasing PAMAM concentration reduces the available Cu^{2+} concentration in the reaction solution; a lower reduction reaction of Cu^{2+} ions leads to less dissolution of Fe and less voids formation. This is why the size and number of the voids decreased with increasing PAMAM concentration. Overall, Cu^{2+} helps the deposition of the Zr-based conversion coating because the reduction of Cu^{2+} changes the hydrogen evolution and oxygen reduction reaction, increasing the local pH value,[29] but also promotes dissolution of metal substrates. The voids may negatively influence the mechanical property of the metal substrates. Incorporation of PAMAM in the conversion coating solutions further provides a tunability to control the contribution of Cu^{2+} ions in the reaction, decreasing the voids formation at the interface between the coating and the substrate.

3.2. Effect of PAMAM on the Internal Microstructure Chemical Distribution of Clusters. The influence of PAMAM on the internal microstructure and chemical distribution of the clusters was characterized by STEM. Figure 2 shows the comparison between samples F-P0 and F-P50,

where F-P50 is a hybrid coating with cluster formation. The coatings formed on thin films were compared with the coatings applied on cold rolled steels under the same conditions (Figure S5), which showed a similar microstructure and elemental distribution. For sample F-P0 (control sample without PAMAM), as shown in Figure 2A and 2B, the cluster contained Zr and Cu. Interestingly, instead of uniform Cu compound clusters, Cu-containing nanoparticles distributed within the clusters, showing a complex microstructure of the clusters. A previous study hypothesized that the cluster was a core−shell structure with Cu covered by Zr.[28] Here, with the help of high-resolution STEM, the structure of the cluster further revealed that nanosized Cu particles distributed within a Zr matrix. For F-P50, the cluster consists of Zr and Cu as well. Similar to F-P0, nanosized Cu distributes in the cluster in F-P50 but in some locations forms a slightly larger (up to tens of nanometers in size) agglomerations (Figure 2C and 2D). For F-P200, the cross-sectional elemental mapping did not show Cu signal in the coating (Figure S6).

The Cu to Zr atomic ratio within the cluster was characterized as shown in Figure S7. Hybrid sample F-P50 had a slightly higher Cu atomic ratio (0.65 for F-P0 and 0.70 for F-P50). Furthermore, the Cu to Zr atomic ratio was quantified as a function of the position from the substrate to the top of the coating as well as laterally across the cluster (Figure 2E and 2F; Figure S8). For F-P0, the Cu to Zr atomic ratio decreased from the bottom to the top, indicating the higher deposition extent of Cu compounds at the early stage of the conversion coating formation. However, for F-P50, the Cu to Zr ratio increased toward the top of the coating. As for quantification of the Cu to Zr atomic ratio laterally across the cluster, both samples had a
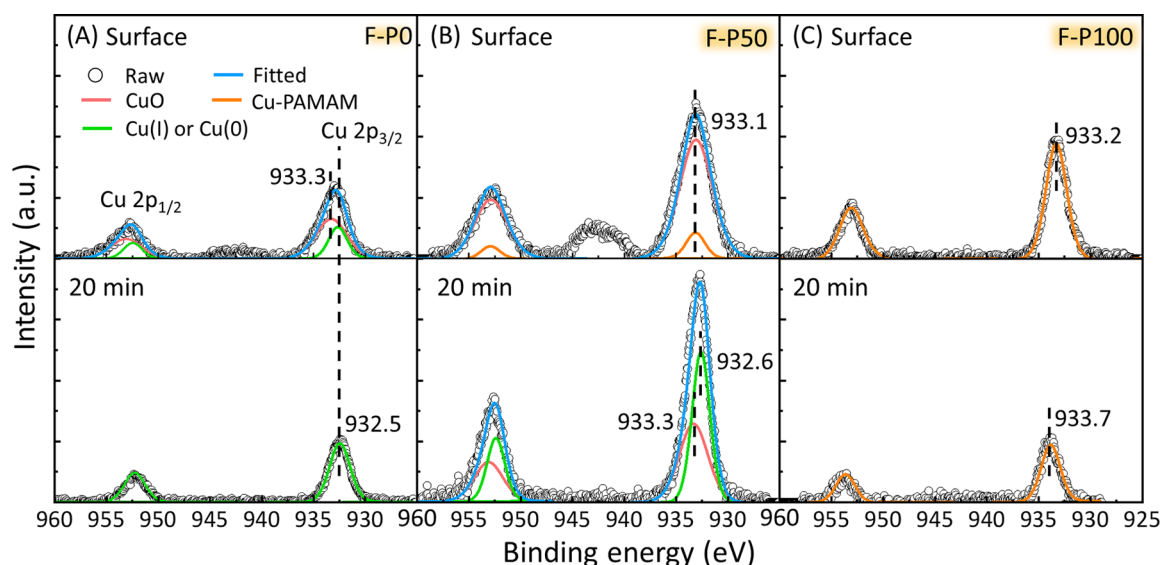
Figure 4. (A−C) Cu 2p fitted XPS spectra of samples F-P0, F-P50, and F-P100 at the surface and 20 min sputtering.

higher Cu to Zr atomic ratio at the center of the cluster. Overall, the region with a higher Cu atomic ratio was mainly at the middle bottom of the cluster for F-P0, whereas the Cu element was concentrated at the middle top of the cluster for F-P100.

3.3. Atomic Ratio Evolution along the Depth Direction, and Chemical Composition of the Coatings. Previous sections mainly discussed the morphology and metal elements' distribution in the coatings. To further understand the coating formation, we analyzed its chemical composition with particular focus on organic compounds in the coating. XPS was used to characterize the change in depth profiles of different elements including Zr, Cu, F, O, C, and N with the varying PAMAM concentrations as well as to identify the chemical compounds.

Figure 3D shows the atomic ratio depth profiling for Zr, Cu, C, and N in different samples. The longer Ar sputtering time in XPS corresponds to further removal of the materials to probe deeper regions in the coating. First, as shown in Figure 3A, when comparing different samples with the same depth, the atomic ratio of Zr decreased with increasing PAMAM concentration with a corresponding increase of the C and N atomic ratio (Figure 3C and 3D), which indicated that the relative ratio of ZrO_2 decreased and the ratio of organic compounds increased with higher PAMAM. As for Cu in Figure 3B, overall the atomic ratio of Cu is relatively low (less than 5 atom %). Specifically, the atomic ratios of Cu for F-P100 and F-P200 were much lower than other samples, meaning a higher PAMAM concentration greatly decreased the ratio of Cu in the coating corresponding to the morphology without Cu-rich clusters. This is likely because formation of the Cu−PAMAM complex consuming most of the Cu^{2+} ions suppressed the cathodic reaction of Cu^{2+}. This indicates that the ability for Cu−PAMAM to be incorporated within the hybrid coatings is lower compared to the deposition of Cu from the reduction reaction of Cu^{2+} ions.

In addition, when examining the atomic ratio as a function of depth for each coating, the atomic ratio of Zr increased initially (0−6 min sputtering time, 0−5 min for F-P100) and became relatively constant for all coating samples. Then for Cu, except for an increase of the atomic ratio from 0 to 2 min, overall the atomic ratio of Cu decreased as a function of depth for all coating samples (Figure 3B). For C, despite the surface C from the

atmosphere, the atomic ratio of C remains stable after 4 min sputtering for samples F-P25 and F-P50 but decreased largely for higher PAMAM samples corresponding to a similar trend as in Cu. This suggests that both XPS signals of Cu and C are from the Cu−PAMAM. The decreasing C and Cu ratios from the surface to the interior region (lower sputtering time) in higher PAMAM samples indicates that there is likely a higher concentration of Cu−PAMAM toward the surface of the coating. Other research suggested that when the amount of Cu is too high in the conversion coating, the coating will become more inhomogeneous, resulting in a poorer protection property of the coating.[16,27] Thus, the PAMAM additive here serves a dual function: (1) it could effectively control the amount of free Cu^{2+} in solution, thereby tuning the electrochemical reactions during coating formation, and (2) it will lead to formation of organic components in the coating.

To further identify the chemical components, high-resolution XPS peak-fitting analysis was carried out on different coating samples. Figure 3E shows the C 1s XPS of sample F-P100 at the surface. The C 1s peak could be deconvoluted into three peaks, corresponding to the carbon atoms in three different functional groups: C−C/C−H (284.8 eV), C−N (285.5 eV), and −N-C═O (288.3 eV).[31,32] The organic groups are associated with PAMAM. Correspondingly, the N 1s peak was deconvoluted into two peaks: positively charged N atoms (401.8 eV) and C−N/ −C-N═O (400.0 eV), as shown in Figure 3F.[33,34] The presence of protonated N is the result of the coordinate covalent bonding with the Cu(II) ions. An electron pair from N could be donated into the vacant orbitals of Cu^{2+} forming donor−acceptor complexes.[35,36] Besides, the Cu 2p XPS peaks for F-P0, F-P50, and F-P100 were deconvoluted to identify the Cu oxidation states at the surface and in the coating (Figure 4A−C, Table S1). The peak of Cu $2p_{3/2}$ was at 933.3 ± 0.1 eV for samples F-P0 and F-P50 at the surface, and there is a satellite peak (~942.0 eV) in the raw data which corresponds to CuO.[37,38] The peak at 932.5 ± 0.1 eV after 20 min sputtering corresponds to Cu(0) or Cu(I). The fitted peak at 933.3 eV for F-P50 after 20 min of sputtering without a satellite peak could be Cu(II) compounds or a lower amount of CuO. The Cu(0) and Cu(I) compounds are the reaction products from cathodic reaction of Cu^{2+} ions, which could be further oxidized to form
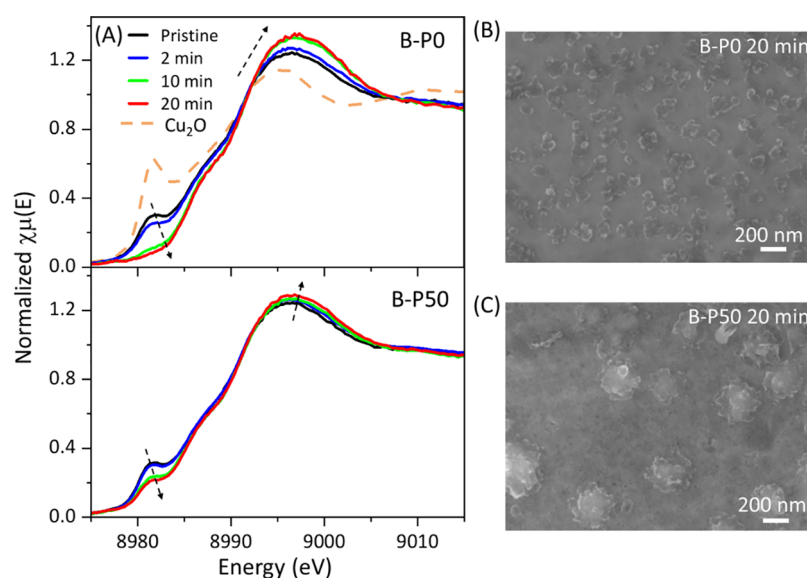
Figure 5. (A) XANES Cu K-edge of samples B-P0 and B-P50 with different treatment times in 0.1 M NaOH solution at 38 °C. (B and C) SEM images show the surface morphology of the samples after treatment for 20 min.

CuO on the surface while in solution or when in contact with air.[39] For F-P100 (20 min sputtering), the main Cu $2p_{3/2}$ peak position shifted to a higher binding energy at 933.7 eV. This peak shift corresponds to the Cu^{2+} ions complexing to amine/amide groups because Cu^{2+} coordinates with a more electronegative atom like the N atom in the amine group.[40] In addition, there is no CuO peak shown on the surface of F-P100. The absence of Cu(0) or Cu(I) peaks means that Cu in the form of a Cu−PAMAM complex is not reduced, indicating the cathodic reaction as well as further oxidation did not occur. Thus, Cu−PAMAM was directly incorporated into the coating. Note that the fitting peak for samples F-P50 and F-P100 at the surface was located at 933.2 ± 0.1 eV. The full width at half-maximum (fwhm) of this peak was different from the CuO peak shown in the F-P0 and F-P50 surfaces with characteristic satellite peaks (Table S1). According to atomic ratio analysis of C and N along the depth direction (Figure 3C and 3D), a higher relative ratio for both elements was observed at the surface of F-P50 and F-P100. Besides, the fwhm of the peak is similar to that of the Cu−PAMAM complex; therefore, this compound could be the Cu−PAMAM complex. However, the peak position slightly shifted to a lower binding energy compared to the Cu−PAMAM complex in coating F-P100. It is possible that other forms of Cu compounds formed due to interaction with air; surface charging may also influence the peak positions. Thus, further characterization is needed to investigate the stability of the Cu−PAMAM complex at the surface of the coating in air, the resulting chemical coordination, and compounds of Cu.

3.4. Surface Morphology and Cu Compositions Change of the Coating in NaOH Solution. In Figure 5A, the Cu K-edge XANES spectrum changed as a function of treatment time in 0.1 M NaOH solution (pH = 12.5) for samples B-P0 and B-P50. Treatment in NaOH solution was to simulate an environment of the E-coat process, which further deposits additional coating layers on top of the chemical conversion coating. The intensity of the pre-edge peak (8890.9 eV) decreased, but the intensity for the postedge peak (∼8996.6 eV) increased and slightly shifted to higher energy as a function of treatment time. The pre-edge peak position was consistent with the standard Cu_2O pre-edge position corresponding to an

electronic transition from 1s to 4p.[41] The decreasing pre-edge peak intensity indicated that Cu_2O in the coating may be dissolved in NaOH solution. Figure 5A shows that the clusters were attacked and dissolved after 20 min of NaOH treatment, comparing to pristine coating (Figure 1B). However, in sample B-P50, the pre-edge peak was still present after NaOH treatment, although with a slight decrease in intensity. The SEM image in Figure 5C still shows apparent cluster features. In addition, the intensity and position of the postedge peak did not change significantly. Hence, incorporation of PAMAM stabilized the clusters in the coating in alkaline solution. With less dissolution of the clusters, less defects or cracks may be introduced during the E-coat deposition. Hence, hybrid coatings with PAMAM will exhibit better chemical stability in an alkaline environment. The chemical stability of the Cu_2O compound as part of the hybrid coating as well as the coating itself in general can be further analyzed.

3.5. Formation Mechanism of the Coating. As it is known that PAMAM has a high density of N and O donors which is applied for removing heavy metal ions such as Cu^{2+}, Pb^{2+}, and Zn^{2+} in aqueous solutions and catalysis.[42,43] Cu could adopt a three, four, five, or six coordination geometry.[44] The pH of the solution and the relative ratio of Cu^{2+} and PAMAM may affect the coordination between the Cu^{2+} and PAMAM. Kotte et al. suggested three classes could form including (1) Cu^{2+} coordinates with four N donors, (2) Cu^{2+} coordinates with two N donors and two O donors, and (3) Cu^{2+} coordinates with six water molecules.[45] Other work done by Diallo et al. suggested another common coordination environment for Cu^{2+} as $[1Cu(II)/2NH_2]$.[46] While the focus of this study is to understand how this Cu−PAMAM complexation influences conversion coating formation, future work could be conducted to reveal further details on the coordination mechanism of Cu and PAMAM.

For the solutions containing Cu^{2+} only and Cu−PAMAM complex, as the Fe substrate is first immersed in solution, the aggressive fluoride ions activate/dissolve the surface. The fluoride ion is related to hexafluorozirconic acid used in this work and will interact with the zirconium oxide layer of the coating. Fluoride ions may also transport through the natural
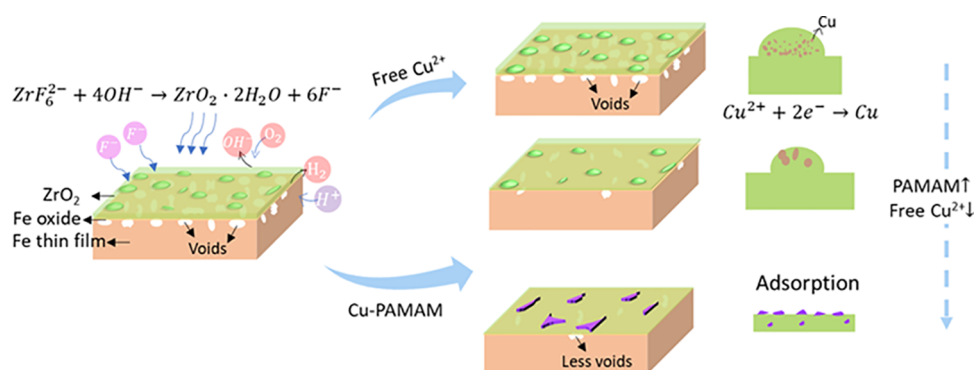
Figure 6. Schematic illustration of the nonhybrid/hybrid coating formation. Here, a moderate amount of Cu deposition is preferred; free Cu^{2+} ions accelerate the dissolution of Fe and form clusters with Cu nanoparticles embedded. This promotes growth of the conversion coating as part of the mechanism. By combining PAMAM and Cu, these reactions could be controlled, leading to less voids, agglomeration of Cu in the cluster, and thinner coating. If Cu^{2+} completely complexes with PAMAM, the adsorption of PAMAM forms a flake-like structure at the outer surface without Cu-containing round clusters formation; this leads to a very thin layer of conversion coating formation and thus is not beneficial.

oxide layer on the surface, etching Fe and forming voids beneath the oxide layer. Then reduction of Cu^{2+} ($Cu^{2+} + 2e^- \rightarrow Cu$) could promote anodic dissolution of Fe as illustrated in Figure 6. However, when PAMAM is added into the solution, the reduction potential of Cu^{2+} complexing with PAMAM is lower than that of pure Cu^{2+} ions;[47,48] then a less cathodic reaction of Cu^{2+} could take place. Thus, in samples formed with higher PAMAM concentration, less void formation and Fe dissolution occurred. If some amount of free Cu^{2+} exists after complexation, the cathodic reaction could still happen and form Cu-containing clusters. On the other hand, if the concentration of PAMAM is high enough to complex all Cu^{2+}, no clusters could form, and instead, flake-like features resulting from the complexation product will be present at the coating surface. Moreover, the cathodic reaction of Cu^{2+} could accelerate the subsequent increase in pH value and precipitation of Zr−hydroxides ($ZrF_6^{2-} + 4OH^- \rightarrow ZrO_2 \cdot 2H_2O + 6F^-$, Figure S9).[12] When the Cu−PAMAM complex forms, this process reduces free Cu^{2+} ions in the coating solution; therefore, the coating will be thinner in samples treated with a higher PAMAM concentration solution. Hence, the incorporation of PAMAM could influence the amount of different chemical reactions (Figure 5) during coating formation and plays an important role in controlling the morphology, thickness, homogeneity, and structure of the coating.

Furthermore, as it is known that PAMAM contains amide and amine groups. Amine could bond to surfaces of transition metal oxides in three different adsorption modes. First, as a transition metal oxide, O in ZrO_2 could transfer a proton acting as a Brønsted acid. The second mode is formation of a bond by sharing the lone pair of electrons from the nitrogen atom with the electron-deficient Zr atom, acting as a Lewis acid site. Last, hydrogen bonding forms through nitrogen interaction with hydrogens on the surface hydroxyl groups or hydrogen from amide with anions.[49,50] Thus, the Cu−PAMAM complex is adsorbed at the surface of the hybrid coatings, forming the flake-like structure (Figure 1) and showing a higher C and N ratio at the surface for hybrid coatings (Figure 3) when Cu complexes with PAMAM completely. Adsorption of PAMAM on ZrO_2 happens in the coating as well. However, for hybrid sample F-P50, Cu 2p XPS does not show coordinated Cu(II). Growth of the ZrO_2 film and surface adsorption of Cu−PAMAM onto the ZrO_2 surface could be competing reactions. When there are free Cu^{2+} ions in solution, deposition of ZrO_2 is promoted; therefore,

less Cu−PAMAM could be adsorbed on ZrO_2 during coating formation. However, when there are no free Cu^{2+} ions in solution, growth of ZrO_2 is suppressed, increasing the probability for Cu−PAMAM adsorption on produced ZrO_2 in the coating. Further research is needed to study the coordination mechanism between Cu(II) and PAMAM in solution and the kinetics of complexation compounds adsorption in the coating.

Overall, the hybrid conversion coating with Cu^{2+} ions and PAMAM presents both functions of inorganic and organic additives. While Cu^{2+} ions affect the deposition kinetics by providing complementary cathodic reaction sites, PAMAM could further control the amount of reduction, dissolution of Fe substrate, and subsequent precipitation reaction of ZrO_2, altering the surface morphology and amount of Cu and Cu compounds of the coating. Moreover, PAMAM could bond to the surface of ZrO_2, increasing adhesion to the subsequent applied organic layer. Thus, adding the proper amount of PAMAM in the Zr-based conversion solution is an effective strategy to improve the performance of the coating.

4. CONCLUSION

The mechanistic effects of organic and inorganic additives on the Zr-based conversion coating are studied. The novel hybrid Zr-based conversion coatings on Fe thin film substrates with varying relative ratios of Cu^{2+} and PAMAM additives were investigated. Multimodal X-ray and electron techniques were utilized to characterize the morphology and chemistry of the coatings. Cu^{2+} for the reduction reaction produces metallic Cu or Cu oxides forming nanosized particles embedded in clusters. As PAMAM is added into solution, Cu−PAMAM complex forms with reduced Cu^{2+} reduction potential. With less free Cu^{2+} in solution, dissolution of Fe, deposition of Cu from the reduction reaction of Cu^{2+}, and growth of ZrO_2 layers decrease, thereby changing the morphology, thickness, elemental (Zr, Cu, C, and N) ratios, and chemical compositions in the coatings. Furthermore, because of the adsorption ability of PAMAM and its incorporation into the coatings (higher concentration toward the surface), the surface of the hybrid coating has an organic compound layer. Moreover, by comparing the Cu K-edge XANES, the hybrid coating shows less change in an alkaline environment with less change of the spectrum and surface morphology.

Both Cu^{2+} and PAMAM have a positive impact on the coating formation mechanism. Cu^{2+} changes the kinetics of the coating

growth, but PAMAM could control the free Cu^{2+} in solution via complexation with Cu^{2+} as well as be adsorbed on the surface of the coating, enhancing adhesion of the subsequent organic coating in multilayer systems. With the proper relative ratio of these two additives, the hybrid Zr-based conversion coating gains advantages from both of them, providing better protection and adhesion performance. As these two additions are nonhazardous and the solution is water based, this work demonstrated an effective, environmentally friendly, and simple method to improve the performance of chemical conversion coatings which plays an important role in substitutions for chromate-free corrosion inhibitors. No extra energy, large cost inputs, and post-treatment steps are needed. More investigation may be conducted to study the complexation mechanism between Cu^{2+} and PAMAM at a molecular level. Essential future work should also provide further understanding on the electrochemical and corrosion behavior of the hybrid coatings via electrochemical techniques such as open-circuit potential measurements as well as cyclic polarization and electrochemical impedance spectroscopy (EIS) analyses.

■ ASSOCIATED CONTENT

ⓢ Supporting Information

The Supporting Information is available free of charge at https://pubs.acs.org/doi/10.1021/acsami.0c19203.

Surface chemical composition of pristine Fe thin film, surface morphology and Cu elemental distribution of F-P50 sample on the surface and cross-section showing Cu-rich clusters, quantification of the size and number density of the clusters as a function of PAMAM concentration, surface morphology of the Zr-based conversion coatings without Cu^{2+} and PAMAM, STEM/EDS maps analysis of the coatings on cold rolled steel substrate, STEM/EDS maps analysis of sample F-P200, Cu to Zr atomic ratio in the clusters in samples F-P0 and F-P50, quantification of the atomic ratio distribution in the surface cluster, fitting parameters of Cu 2p3/2 XPS in samples F-P0, F-P50 and F-P100 and surface Zr XPS peaks of different samples (PDF)

■ AUTHOR INFORMATION

Corresponding Author

Yu-chen Karen Chen-Wiegart − *Department of Materials Science and Chemical Engineering, Stony Brook University, Stony Brook, New York 11794, United States; National Synchrotron Light Source II, Brookhaven National Laboratory, Upton, New York 11973, United States;* ⓞ orcid.org/0000-0003-4445-2159; Email: Karen.Chen-Wiegart@stonybrook.edu

Authors

Xiaoyang Liu − *Department of Materials Science and Chemical Engineering, Stony Brook University, Stony Brook, New York 11794, United States;* ⓞ orcid.org/0000-0002-9326-2135

Donald Vonk − *Henkel Corporation, Madison Heights, Michigan 48071, United States*

Kim Kisslinger − *Center for Functional Nanomaterials, Brookhaven National Laboratory, Upton, New York 11973, United States*

Xiao Tong − *Center for Functional Nanomaterials, Brookhaven National Laboratory, Upton, New York 11973, United States*

Gary Halada − *Department of Materials Science and Chemical Engineering, Stony Brook University, Stony Brook, New York 11794, United States*

Stanislas Petrash − *Henkel Corporation, Bridgewater, New Jersey 08807, United States*

Kate Foster − *Henkel Corporation, Madison Heights, Michigan 48071, United States*

Complete contact information is available at:
https://pubs.acs.org/10.1021/acsami.0c19203

Notes

The authors declare no competing financial interest.

■ ACKNOWLEDGMENTS

■ REFERENCES

(1) Tran, T. H.; Vimalanandan, A.; Genchev, G.; Fickert, J.; Landfester, K.; Crespy, D.; Rohwerder, M. Regenerative Nano-Hybrid Coating Tailored for Autonomous Corrosion Protection. *Adv. Mater.* **2015**, *27* (25), 3825−3830.

(2) Zheludkevich, M. L.; Shchukin, D. G.; Yasakau, K. A.; Mohwald, H.; Ferreira, M. G. S. Anticorrosion Coatings with Self-healing Effect Based on Nanocontainers Impregnated with Corrosion Inhibitor. *Chem. Mater.* **2007**, *19* (3), 402−411.

(3) Prasai, D.; Tuberquia, J. C.; Harl, R. R.; Jennings, G. K.; Bolotin, K. I. Graphene: Corrosion-Inhibiting Coating. *ACS Nano* **2012**, *6* (2), 1102−1108.

(4) Lee, J.; Shin, S.; Jiang, Y. H.; Jeong, C.; Stone, H. A.; Choi, C. H. Oil-Impregnated Nanoporous Oxide Layer for Corrosion Protection with Self-Healing. *Adv. Funct. Mater.* **2017**, *27* (15), 1606040.

(5) Sekularac, G.; Kovac, J.; Milosev, I. Prolonged Protection, by Zirconium Conversion Coatings, of AlSi7Mg0.3 Aluminium Alloy in Chloride Solution. *Corros. Sci.* **2020**, *169*, 108615.

(6) Gheytani, S.; Liang, Y. L.; Jing, Y.; Xu, J. Q.; Yao, Y. Chromate Conversion Coated Aluminium as A Lightweight and Corrosion-Resistant Current Collector for Aqueous Lithium-Ion Batteries. *J. Mater. Chem. A* **2016**, *4* (2), 395−399.

(7) Shchukin, D. G.; Zheludkevich, M.; Yasakau, K.; Lamaka, S.; Ferreira, M. G. S.; Mohwald, H. Layer-by-layer Assembled Nano-containers for Self-Healing Corrosion Protection. *Adv. Mater.* **2006**, *18* (13), 1672.

(8) Adhikari, S.; Unocic, K. A.; Zhai, Y.; Frankel, G. S.; Zimmerman, J.; Fristad, W. Hexafluorozirconic Acid based Surface Pretreatments: Characterization and Performance Assessment. *Electrochim. Acta* **2011**, *56* (4), 1912−1924.

(9) Fix, D.; Andreeva, D. V.; Lvov, Y. M.; Shchukin, D. G.; Moehwald, H. Application of Inhibitor-Loaded Halloysite Nanotubes in Active

Anti-Corrosive Coatings. *Adv. Funct. Mater.* **2009**, *19* (11), 1720−1727.

(10) Zhou, W. Q.; Shan, D. Y.; Han, E. H.; Ke, W. Structure and Formation Mechanism of Phosphate Conversion Coating on Die-Cast AZ91D Magnesium Alloy. *Corros. Sci.* **2008**, *50* (2), 329−337.

(11) Gharbi, O.; Thomas, S.; Smith, C.; Birbilis, N. Chromate Replacement: What Does the Future Hold? *npj Mater. Degrad.* **2018**, *2*, 2−12.

(12) Milosev, I.; Frankel, G. S. Review-Conversion Coatings Based on Zirconium and/or Titanium. *J. Electrochem. Soc.* **2018**, *165*, C127−C144.

(13) Giles, T. R.; Vonk, D.; Favero, S.-L. The Next Generation of Conversion Coatings; Henkel Corporation, 2012.

(14) Taheri, P.; Lill, K.; de Wit, J. H. W.; Mol, J. M. C.; Terryn, H. Effects of Zinc Surface Acid-Based Properties on Formation Mechanisms and Interfacial Bonding Properties of Zirconium-Based Conversion Layers. *J. Phys. Chem. C* **2012**, *116* (15), 8426−8436.

(15) Li, L. L.; Whitman, B. W.; Swain, G. M. Characterization and Performance of a Zr/Ti Pretreatment Conversion Coating on AA2024-T3. *J. Electrochem. Soc.* **2015**, *162* (6), C279−C284.

(16) Lostak, T.; Krebs, S.; Maljusch, A.; Gothe, T.; Giza, M.; Kimpel, M.; Flock, J.; Schulz, S. Formation and Characterization of Fe3+-/Cu2+-Modified Zirconium Oxide Conversion Layers on Zinc Alloy Coated Steel Sheets. *Electrochim. Acta* **2013**, *112*, 14−23.

(17) Liu, X.; Vonk, D.; Jiang, H.; Kisslinger, K.; Tong, X.; Ge, M.; Nazaretski, E.; Ravel, B.; Foster, K.; Petrash, S.; Chen-Wiegart, Y.-c. K. Environmentally Friendly Zr-Based Conversion Nanocoatings for Corrosion Inhibition of Metal Surfaces Evaluated by Multimodal X-ray Analysis. *Acs Appl. Nano Mater.* **2019**, *2*, 1920.

(18) Zhu, W.; Li, W. F.; Mu, S. L.; Yang, Y. Y.; Zuo, X. The Adhesion Performance of Epoxy Coating on AA6063 Treated in Ti/Zr/V Based Solution. *Appl. Surf. Sci.* **2016**, *384*, 333−340.

(19) Vonk, D. R.; Smith, T. S., II; Bobadilla, A. Thin Corrosion Protective Coatings Incorporating Polyamidoamine Polymers. US Patent 20180037770, Feb. 8, 2018.

(20) Vonk, D. R.; Smith, T. S., II; Bobadilla, A. Thin Corrosion Protective Coatings Incorporating Polyamidoamine Polymers. WO/2016/167928, Feb 8, 2018.

(21) Shmueli, Y.; Lin, Y. C.; Lee, S.; Zhernenkov, M.; Tannenbaum, R.; Marom, G.; Rafailovich, M. H. In Situ Time-Resolved X-ray Scattering Study of Isotactic Polypropylene in Additive Manufacturing. *ACS Appl. Mater. Interfaces* **2019**, *11* (40), 37112−37120.

(22) Zou, L. J.; Ge, M. Y.; Zhao, C. H.; Meng, Q. K.; Wang, H.; Liu, X. Y.; Lin, C. H.; Xiao, X. H.; Lee, W. K.; Shen, Q.; Chen, F.; Chen-Wiegart, Y. C. K. Designing Multiscale Porous Metal by Simple Dealloying with 3D Morphological Evolution Mechanism Revealed via X-ray Nano-tomography. *ACS Appl. Mater. Interfaces* **2020**, *12* (2), 2793−2804.

(23) Cunha, G. D.; Peixoto, J. A.; de Souza, D. R.; Romao, L. P. C.; Macedo, Z. S. Recycling of Chromium Wastes from the Tanning Industry to Produce Ceramic Nanopigments. *Green Chem.* **2016**, *18* (19), 5342−5356.

(24) Weiland, C.; Jaye, C.; Quackenbush, N. F.; Gann, E.; Fu, Z.; Kirkland, J. P.; Karlin, B. A.; Ravel, B.; Woicik, J. C.; Fischer, D. A. NIST HAXPES at NSLS and NSLS-II. *Synchrotron Radiation News* **2018**, *31* (4), 23.

(25) Basnet, P.; Larsen, G. K.; Jadeja, R. P.; Hung, Y. C.; Zhao, Y. P. alpha-Fe2O3 Nanocolumns and Nanorods Fabricated by Electron Beam Evaporation for Visible Light Photocatalytic and Antimicrobial Applications. *ACS Appl. Mater. Interfaces* **2013**, *5* (6), 2085−2095.

(26) Diallo, M. S.; Christie, S.; Swaminathan, P.; Balogh, L.; Shi, X. Y.; Um, W.; Papelis, C.; Goddard, W. A.; Johnson, J. H. Dendritic Chelating Agents. 1. Cu(II) Binding to Ethylene Diamine Core Poly(amidoamine) Dendrimers in Aqueous Solutions. *Langmuir* **2004**, *20* (7), 2640−2651.

(27) Vonk, D. R.; Kapic, E.; Sienkowski, M. L. Metal Pretreatment Composition Containing Zirconium, Copper, and Metal Chelating Agents and Related Coatings on Metal Substrates. US 9,580,813B2, Feb 28, 2017.

(28) Cerezo, J.; Vandendael, I.; Posner, R.; de Wit, J. H. W.; Mol, J. M. C.; Terryn, H. The Effect of Surface Pre-conditioning Treatments on the Local Composition of Zr-based Conversion Coatings Formed on Aluminium Alloys. *Appl. Surf. Sci.* **2016**, *366*, 339−347.

(29) Cerezo, J.; Vandendael, I.; Posner, R.; Lill, K.; de Wit, J. H. W.; Mol, J. M. C.; Terryn, H. Initiation and Growth of Modified Zr-based Conversion Coatings on Multi-Metal Surfaces. *Surf. Coat. Technol.* **2013**, *236*, 284−289.

(30) Valand, T.; Nilsson, G. The Influence of F- Ions on the Electrochemical Reactions on Oxide-Covered A1. *Corros. Sci.* **1977**, *17* (6), 449−459.

(31) Ma, L.; Zhuang, H. L. L.; Wei, S. Y.; Hendrickson, K. E.; Kim, M. S.; Cohn, G.; Hennig, R. G.; Archer, L. A. Enhanced Li-S Batteries Using Amine-Functionalized Carbon Nanotubes in the Cathode. *ACS Nano* **2016**, *10* (1), 1050−1059.

(32) Xue, S. M.; Xu, Z. L.; Tang, Y. J.; Ji, C. H. Polypiperazine-amide Nanofiltration Membrane Modified by Different Functionalized Multiwalled Carbon Nanotubes (MWCNTs). *ACS Appl. Mater. Interfaces* **2016**, *8* (29), 19135−19144.

(33) Cohen, A.; Yang, Y. Z.; Yan, Q. L.; Shlomovich, A.; Petrutik, N.; Burstein, L.; Pang, S. P.; Gozin, M. Highly Thermostable and Insensitive Energetic Hybrid Coordination Polymers Based on Graphene Oxide-Cu(II) Complex. *Chem. Mater.* **2016**, *28* (17), 6118−6126.

(34) Wang, X. Q.; Liu, C. G.; Neff, D.; Fulvio, P. F.; Mayes, R. T.; Zhamu, A.; Fang, Q.; Chen, G. R.; Meyer, H. M.; Jang, B. Z.; Dai, S. Nitrogen-Enriched Ordered Mesoporous Carbons through Direct Pyrolysis in Ammonia with Enhanced Capacitive Performance. *J. Mater. Chem. A* **2013**, *1* (27), 7920−7926.

(35) Fiorillo, A. A.; Galbraith, J. M. A Valence Bond Description of Coordinate Covalent Bonding. *J. Phys. Chem. A* **2004**, *108* (23), 5126−5130.

(36) Timoshkin, A. Y.; Frenking, G. Low-Valent Group-13 Chemistry. Theoretical Investigation of the Structures and Relative Stabilities of Donor-Acceptor Complexes R3E-E′R′ and Their Isomers (RE)-E-2-E′RR′. *J. Am. Chem. Soc.* **2002**, *124* (24), 7240−7248.

(37) Chen, S. S.; Brown, L.; Levendorf, M.; Cai, W. W.; Ju, S. Y.; Edgeworth, J.; Li, X. S.; Magnuson, C. W.; Velamakanni, A.; Piner, R. D.; Kang, J. Y.; Park, J.; Ruoff, R. S. Oxidation Resistance of Graphene-Coated Cu and Cu/Ni Alloy. *ACS Nano* **2011**, *5* (2), 1321−1327.

(38) Pal, J.; Mondal, C.; Sasmal, A. K.; Ganguly, M.; Negishi, Y.; Pal, T. Account of Nitroarene Reduction with Size- and Facet-Controlled CuO-MnO2 Nanocomposites. *ACS Appl. Mater. Interfaces* **2014**, *6* (12), 9173−9184.

(39) Sarfraz, A.; Posner, R.; Lange, M. M.; Lill, K.; Erbe, A. Role of Intermetallics and Copper in the Deposition of ZrO2 Conversion Coatings on AA6014. *J. Electrochem. Soc.* **2014**, *161* (12), C509−C516.

(40) Terra, J. C. S.; Moores, A.; Moura, F. C. C. Amine-Functionalized Mesoporous Silica as a Support for on-Demand Release of Copper in the A(3)-Coupling Reaction: Ultralow Concentration Catalysis and Confinement Effect. *ACS Sustainable Chem. Eng.* **2019**, *7* (9), 8696−8705.

(41) Ravel, B.; Carr, G. L.; Hauzenberger, C. A.; Klysubun, W. X-ray and Optical Spectroscopic Study of the Coloration of Red Glass Used in 19th Century Decorative Mosaics at the Temple of the Emerald Buddha. *J. Cult. Herit* **2015**, *16* (3), 315−321.

(42) Crooks, R. M.; Zhao, M. Q.; Sun, L.; Chechik, V.; Yeung, L. K. Dendrimer-Encapsulated Metal Nanoparticles: Synthesis, Characterization, and Applications to Catalysis. *Acc. Chem. Res.* **2001**, *34* (3), 181−190.

(43) Zhang, Q.; Wang, N.; Zhao, L. B.; Xu, T. W.; Cheng, Y. Y. Polyamidoamine Dendronized Hollow Fiber Membranes in the Recovery of Heavy Metal Ions. *ACS Appl. Mater. Interfaces* **2013**, *5* (6), 1907−1912.

(44) Liu, F. Q.; Li, L. J.; Ling, P. P.; Jing, X. S.; Li, C. H.; Li, A. M.; You, X. Z. Interaction Mechanism of Aqueous Heavy Metals onto A Newly Synthesized IDA-Chelating Resin: Isotherms, Thermodynamics and Kinetics. *Chem. Eng. J.* **2011**, *173* (1), 106−114.

(45) Kotte, M. R.; Kuvarega, A. T.; Cho, M.; Mamba, B. B.; Diallo, M. S. Mixed Matrix PVDF Membranes With in Situ Synthesized PAMAM Dendrimer-Like Particles: A New Class of Sorbents for Cu(II) Recovery from Aqueous Solutions by Ultrafiltration. *Environ. Sci. Technol.* **2015**, *49* (16), 9431−9442.

(46) Diallo, M. S.; Balogh, L.; Shafagati, A.; Johnson, J. H.; Goddard, W. A.; Tomalia, D. A. Poly(amidoamine) Dendrimers: A New Class of High Capacity Chelating Agents for Cu(II) Ions. *Environ. Sci. Technol.* **1999**, *33* (5), 820−824.

(47) Bhatt, V. *Essentials of Coordination Chemistry*; Elsevier: 2016; p 282.

(48) Rakshit, A.; Khatua, K.; Shanbhag, V.; Comba, P.; Datta, A. Cu2+ Selective Chelators Relieve Copper-Induced Oxidative Stress in Vivo. *Chemical Science* **2018**, *9* (41), 7916−7930.

(49) Arce-Ramos, J.-M.; Grabow, L. C.; Handy, B. E.; Cardenas-Galindo, M.-G. Nature of Acid Sites in Silica-Supported Zirconium Oxide: A Combined Experimental and Periodic DFT Study. *J. Phys. Chem. C* **2015**, *119* (27), 15150−15159.

(50) Bhatti, U. H.; Nam, S.; Park, S.; Baek, I. H. Performance and Mechanism of Metal Oxide Catalyst-Aided Amine Solvent Regeneration. *ACS Sustainable Chem. Eng.* **2018**, *6* (9), 12079−12087.